Electronic Supporting Information

Construction of hierarchical porous and polydopamine/salicylaldoxime functional zeolitic imidazolate framework-8 via controlled etching for uranium adsorption

Kai Tuo,[a] Jin Li,[a] Yi Li,[a] Chuyao Liang,[a] Cuicui Shao,[a] Weifeng Hou,[a] Zhijian Li,*[a] Shouzhi Pu,*[b] Chunhui Deng*[c]

Kai Tuo, Jin Li, Yi Li, Chuyao Liang, Cuicui Shao, Weifeng Hou, Congbin Fa, Gang Liu, Zhijian Li

[a] *Jiangxi Key Laboratory of Organic Chemistry, Jiangxi Science and Technology Normal University, Nanchang 330013, PR China*

E-mail: lizhijianhdd@163.com

Shouzhi Pu

[b] *YuZhang Normal University, Nanchang 330013, PR China*

E-mail: pushouzhi@tsinghua.org.cn

[c] *Chunhui Deng*

Shanghai Pudong Hospital, and Department of Chemistry, Fudan University，Shanghai 201399,China.

E-mail: chdeng@fudan.edu.cn.

Experimental Saction

1. Materials and Reagents

All reagents were of analytical grade and obtained from commercial suppliers without further purification. Zinc nitrate hexahydrate ($Zn(NO)_3 \cdot 6H_2O$), 2-methylimidazole (2-MeIM), dopamine hydrochloride (DA), ethylenediaminetetraacetic acid disodium (EDTA), salicylaldoxime, uranyl nitrate hexahydrate ($UO_2(NO_3)_2 \cdot 6H_2O$), sodium chloride (NaCl), calcium chloride anhydrous ($CaCl_2$), magnesium sulfate ($MgSO_4$), potassium chloride (KCl), sodium sulfate anhydrous (Na_2SO_4), sodium carbonate anhydrous (Na_2CO_3), tetrabutylammonium fluoride hydrateiron (III) nitrate nonahydrate ($Fe(NO_3)_3 \cdot 9H_2O$), copper nitrate trihydrate ($Cu(NO_3)_2 \cdot 3H_2O$), lead(II) nitrate ($Pb(NO_3)_2$), cobalt nitrate hexahydrate ($Co(NO_3)_2 \cdot 6H_2O$), barium nitrate ($Ba(NO_3)_2$), sodium metavanadate ($NaVO_3$), sodium perchlorate monohydrate ($NaClO_4 \cdot H_2O$), ethanol (EtOH), were purchased from Innochem Science and Technology Co., Ltd (Beijing, China). The bacterial strains of Gram-negative *Escherichia coli (E. coli*), Gram-positive *Staphylococcus aureus* (*S. aureus*), and liquid Luria broth (LB) were provided by Beijing Microbiological Culture collection Center.

2. Instrumentation

Fourier transform infrared (FT-IR) spectra were received on a Nicolet Fourier spectrophotometer (U.S.A) using KBr pellets. Powder X-ray diffraction (PXRD) patterns were evaluated on Rigaku D/max-2500 X-ray diffractometer with Cu Kα radiation. Scanning electron microscopy (SEM) was taken from a Philips-FEI Tecnai G2S-Twin microscope operated at 200 kV acceleration voltages. The morphology was obtained FEI Tecnai F20 (Thermo, America) transmission electron microscope (TEM). The N_2 adsorption-desorption isotherms were characterized to explore the surface area and porous nature by a surface area analyzer (ASAP 2460). Thermogravimetric analysis (TGA) was measured on a Netzsch Tarsus 209F3 system with a heating rate of 2 °C min^{-1} from room temperature to 600 °C under air atmosphere. The water contact angles were measured on a Dataphysics OCA20 contact-angle system at room temperature.

Zeta potentials were obtained via a Nano Is Malvern Zetasizer (UK). The UV-Vis absorption spectra were obtained with an Agilent 8453 UV-Vis spectrophotometer. X-ray photoelectron spectroscopy (XPS) was conducted using Axis Ultra DLD spectrometer (Kratos Analytical Ltd, Britain). Inductively coupled plasma mass spectrometry (ICP-MS) experiments were performed on an Agilent 7700 instrument. Inductively Coupled Plasma Optical Emission Spectrometer (ICP-OES) was performed using an Agilent720ES instrument.

3. Experimental procedures

3.1. Synthesis of ZIF-8

ZIF-8 was prepared according to previous research.[1] Zn $(NO)_3 \cdot 6H_2O$ (35.7 mg) was added to 400 μL deionized water (DI) and will be used as a metal precursor solution. Subsequently, metal precursor solution was added to an aqueous solution of 2-MeIM (1.25 M, 2.6 mL), and by continuous stirring at 400 rpm for 30 min at room temperature. After that, the resultant solidification was collected by centrifugation at 8000 rpm for 2 min and washed with DI three times. At last, ZIF-8 was obtained after drying for 10 h at 50 ℃ under vacuum.

3.2. Synthesis of PDA/SA-ZIF-8

Zn $(NO_3)_2 \cdot 6H_2O$ (89.2 mg) was dispersed in 10 mL DI. Then, 19 mg DA and 19 mg salicylaldoxime were added to the Zn $(NO)_3 \cdot 6H_2O$ aqueous solution at the same time. After that, the above solution was added to the 10 mL of 2-MeIM solution by drops, kept by magnetic stirring at room temperature for 2 h. The PDA/SA-ZIF-8 was collected by centrifugation at 8000 rpm for 2 min washed with DI water three times. The control experiments proceeded as the above synthesis steps with a varied mass ratios of DA/salicylaldoxime (1:0.5, 1:1, 1:2, 1:4) while other parameters remained unchanged.

3.3. Synthesis of H-PDA/SA-ZIF-8

The H-PDA/SA-ZIF-8 was prepared by etching in a controlled manner with an EDTA solution. The PDA/SA-ZIF-8 (60 mg) was brought into a 25 mL round-bottomed flask, and EDTA solution (25 mM, 8 mL) was poured slowly into the flask, the mixture was sonicated for 1 min to form a homogeneous mixture and stirred (500 rpm) slowly

at room temperature. To ensure proper etching, the EDTA solution was refreshed at different time intervals (5 min, 10 min, 20 min, 40 min). The resultant reaction solution was then extracted and subjected to centrifugation at 8000 rpm for 1 min. Subsequently, the sample was washed thrice with DI water.

3.4. Uranium adsorption experiments

To study the uranium adsorption properties of the H-PDA/SA-ZIF-8, the influence of the ratio of adsorbent to solution, pH of the uranium solution, contact time, initial uranium concentration, adsorption temperature, and ionic strength interfering ions were all investigated. The pH values of solution were adjusted to 3-8 with 0.1 M HCl and 0.1 M NaOH. 0.05 g L^{-1} adsorbent was dispersed in 25 mL uranium-spiked deionized water and the mixture was introduced into a conical flask in a 24 h thermostatic shaker bath. The concentrations of uranium in the solution were determined via UV–Vis absorption spectra on the basis of the specific peak at 656 nm for the complexation between Arsenazo(III) chromogenic agent and uranyl, after filtered through 0.22 μm filter membrane. The uranium removal rate and adsorption capacity on the adsorbent could be calculated using Equation (1) and Equation (2):

$$removal\ rate\ (\%) = \frac{C_0 - C_t}{C_0} \times 100\% \quad (1)$$

where C_0 (mg L^{-1}) represents the initial concentrations of uranium and C_t (mg L^{-1}) is the concentrations of uranium at time t.

$$q_e = (C_o - C_t)V/m \quad (2)$$

Where q_e (mg g^{-1}) is the equilibrium adsorption capacity of uranium. C_0 (mg L^{-1}) represents the initial concentrations of uranium and C_t (mg L^{-1}) is the concentrations of uranium at time t. V (L) is volume of the reaction system, and m (g) is the amount of adsorbent.

To investigate the effect of high concentration ions on uranium adsorption in seawater, 0.01 mol L^{-1}cations (Na^+, K^+, Ca^{2+}, and Mg^{2+}) and anions (Cl^-, F^-, SO_4^{2-}, and CO_3^{2-}) were added to the 20 ppm uranium solution, respectively.

3.5. Adsorption kinetics, isotherms, and thermodynamics models

The linear shapes of pseudo-first-order (PFO) and pseudo-second-order (PSO) models were expressed as Equation (3) and Equation (4):

$$\ln\left(q_e - q_t\right) = lnq_e - k_1 t \quad (3)$$

$$\frac{t}{q_t} = \frac{t}{q_e} + \frac{1}{k_2 q_e^2} \quad (4)$$

Where q_t (mg g^{-1}) and q_e (mg g^{-1}) are the adsorption capacity at any time t (min) and the equilibrium adsorption capacity of uranium. k_1 (min^{-1}) represents the equilibrium rate constant of the pseudo first-order sorption. k_2 (g mg^{-1} min^{-1}) represents the equilibrium rate constant of the pseudo second-order sorption.

The fitting equations of the Langmuir model and Freundlich model were shown in Equation (5) and Equation (6), respectively.

$$\frac{C_e}{q_e} = \frac{1}{Q_m k_L} + \frac{C_e}{Q_m} \quad (5)$$

$$lnq_e = lnk_F + \frac{1}{n} lnC_e \quad (6)$$

Where C_e (mg L^{-1}) and q_e (mg g^{-1}) are the equilibrium concentration of uranium and the equilibrium adsorption capacity of uranium. Q_m (mg g^{-1}) is the theoretical maximum adsorption capacity of uranium adsorbed per unit mass of samples. k_L (L mg^{-1}) is the constant related to the Langmuir adsorption, and k_F is the constant related to the Freundlich adsorption. 1/n is an empirical parameter corresponding to surface heterogeneity or adsorption intensity.

The thermodynamic parameters were calculated by using the following Equation (7), Equation (8), and Equation (9)：

$$K_c = \frac{q_e}{C_e} \quad (7)$$

$$lnK_c = \frac{\Delta S^0}{R} - \frac{\Delta H^0}{RT} \quad (8)$$

$$\Delta G^0 = - RTlnK_c \quad (9)$$

where R is the gas constant (8.314 J mol^{-1} K^{-1}), T (K) is the absolute temperature, and K_C is the adsorption equilibrium constant. The thermodynamic parameters were calculated from the plots of ln K_C versus 1/T.

3.6. Adsorption selectivity and reusability

The adsorption selectivity of the H-PDA/SA-ZIF-8 towards uranium was investigated in the presence of multiple coexisting metal ions in simulated seawater. The concentrations of U, V, Cu, Pb, Zn, and Co were 100 times those in natural seawater. The concentrations of Fe and Ba were about 10 times higher than those in natural seawater (Table S5). The pH value was adjusted to 8.0 using 0.1 M NaOH. Subsequently, 0.05 g L^{-1} of the H-PDA/SA-ZIF-8 was shaken for 24 h at 25 °C to achieve sorption equilibrium. Then the solid sorbent was filtered through a 0.22 μm membrane filter and the remaining concentration for different ions were determined by ICP-MS. The selective adsorption performance of the H-PDA/SA-ZIF-8 for uranium was evaluated by using the following Equation (10):

$$K_d = \frac{(C_0 - C_e)V}{C_e m} \times 1000 \quad (10)$$

where K_d value is the dispersion coefficient (mL g^{-1}), V is volume of the reaction system (mL), m is the amount of adsorbent (mg), C_0 (mg L^{-1}) represents the initial concentrations of uranium and C_t (mg L^{-1}) is the concentrations of uranium at time t.

Five consecutive adsorption-desorption cycles were performed to study the reusability of H-PDA/SA-ZIF-8. 0.05 g L^{-1} of H-PDA/SA-ZIF-8 was added into 5 ppm uranium-spiked deionized water and stirred at 130 rpm for 24 h at 25 °C in each adsorption cycle, and then the uranium-loaded material was collected by high-speed centrifuge. The supernatant was filtered by a 0.22 μm nylon membrane filter and the residual concentration of uranium was determined by UV–Vis absorption spectra. The adsorption capacity of material for uranium was calculated using Equation 4. In the desorption experiment, the uranium-loaded material was then regenerated by immersion in an eluent (25 mL of 0.1 M HCl solution) with stirring for 1h. After elution, the material was regenerated in an alkaline solution (20 mL of 5mM NaOH) for 15 min and then used for the next cycle.

3.7. Adsorption tests in seawater

Seawater was collected from the South China Sea near the Shenzhen City, Guangdong Province. The module with 1.5 mg H-PDA/SA-ZIF-8 was used to treat 5 L seawater at the flow rate of 16 mL min^{-1} for 15 days at room temperature. Seawater samples were taken at 1, 3, 6, 10 and 15 days and filtered using a 0.22 μm nylon membrane. The adsorption capacity was determined according to the ICP−MS analysis of the U content and calculated using eq 2.

3.8. Theoretical calculations

The quantum chemical calculations were performed using DFT method within Gaussian 09 package. The equilibrium geometries were calculated by the hybrid exchange-correlation function Becke three parameters hybrid exchange-correlation functional (B3LYP). During structure optimization, the Stuttgart–Dresden–Bonn relativistic effective core potentials (SDD) were applied for uranium, and the basis set of 6–31 G(d) was chosen for the other light atoms C, H, O, and N atoms. The solvation effects were considered by the polarizable continuum model (PCM), which simulated the solvation effect in aqueous solution. The adsorption energies of UO_2^{2+} with H-PDA/SA-ZIF-8 are computed as following:

$$E_{ads} = E_{total} - E_{substrate} - E_{UO_2^{2+}} \quad (11)$$

3.9. Antibacterial activity test

The antibacterial performance of the H-PDA/SA-ZIF-8 toward *E. coli* and *S. aureus* was measured according to predecessor's research.[2,3] The bacterial suspension with H-PDA/SA-ZIF-8 in a constant temperature shaker at 37 ℃ for 12 h, the inhibition of H-PDA/SA-ZIF-8 on the growth curve of *E. coli* and *S. aureus* were evaluated according to OD_{600} at different time (1 h, 2 h, 4 h, 6 h, 8 h, 12 h). 0.3 mL of the bacterial solution was evenly spread on the culture medium and placed at 37 ℃ for 24 h. The contrasted experiments were also performed without H-PDA/SA-ZIF-8.

4. Characterization of H-PDA/SA-ZIF-8

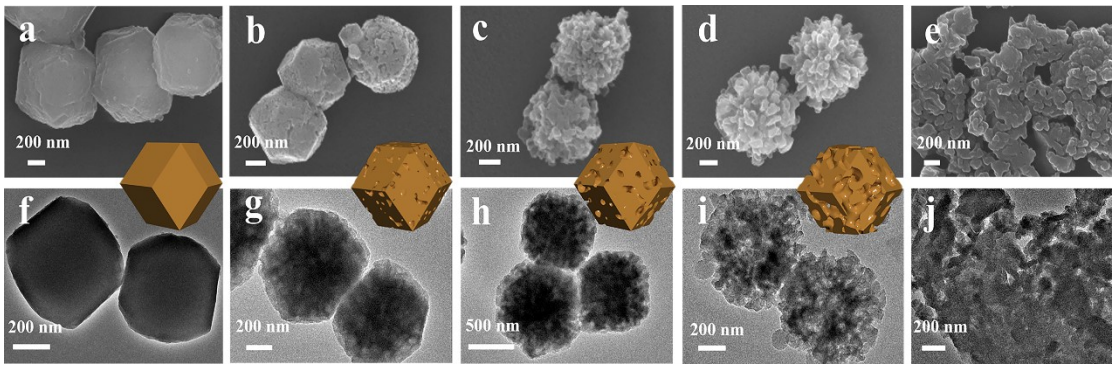

Fig. S1 (a) SEM images of ZIF-8, and H-PDA/SA-ZIF-8 with increasing EDTA etching time: (b) 5 min, (c) 10 min, (d) 20 min, (e) 40 min, respectively. (f) TEM images of PDA/SA-ZIF-8, and H-PDA/SA-ZIF-8 with increasing EDTA etching time: (g) 5 min, (h) 10 min, (i) 20 min, (j) 40 min, respectively.

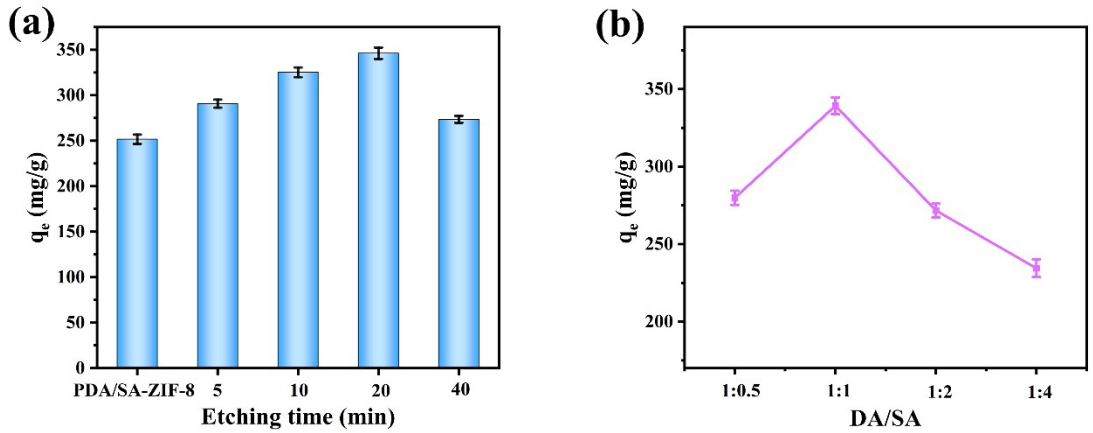

Fig. S2 (a) Effect of different etching time on adsorption capacity, (b) adsorption capability of the H-PDA/SA-ZIF-8 prepared by different additional amounts of salicylaldoxime.

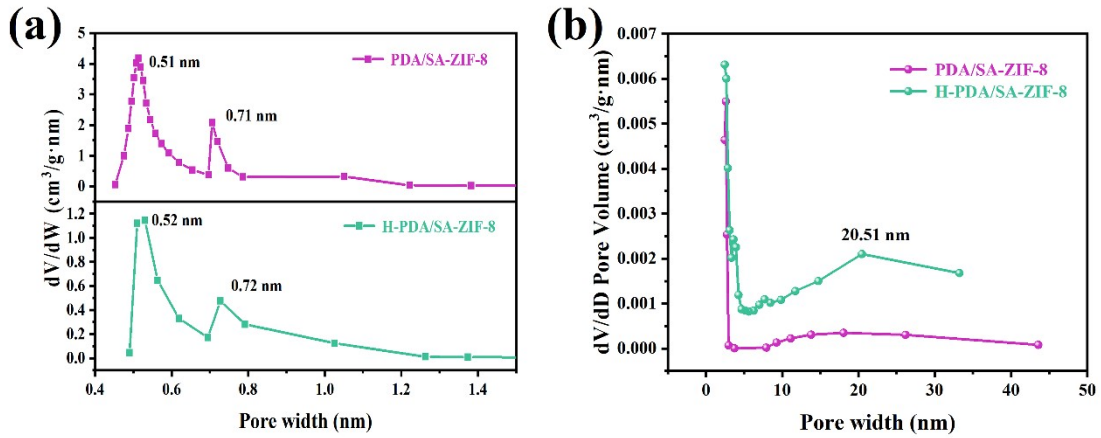

Fig. S3 Pore size distribution of PDA/SA-ZIF-8 and H-PDA/SA-ZIF-8 based on HK model (a) and BJH model.

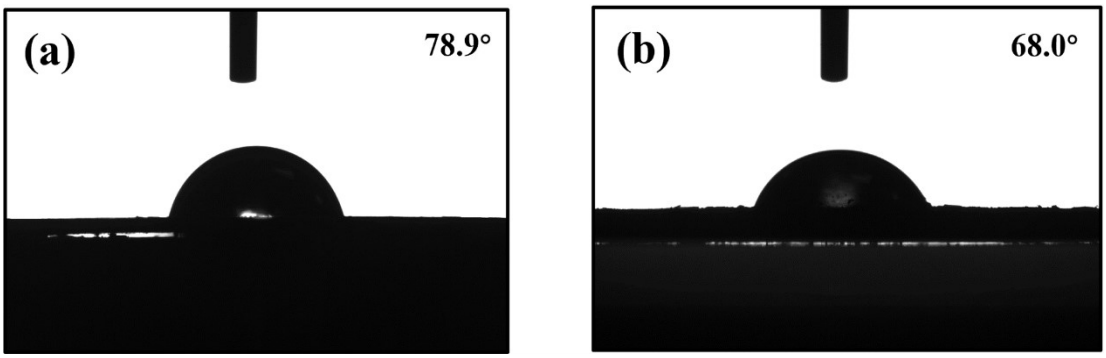

Fig. S4 (a) Water contact angle measurement of PDA/SA-ZIF-8 and (b) H-PDA/SA-ZIF-8.

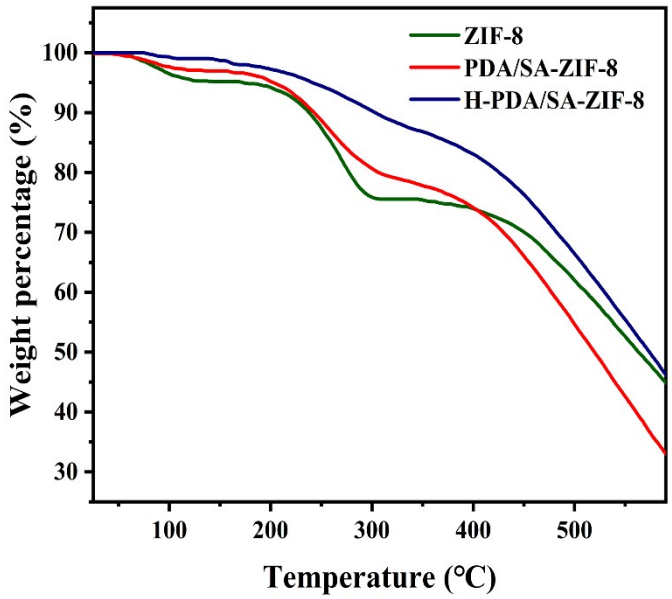

Fig. S5 The TGA curve of ZIF-8, PDA/SA-ZIF-8, and H-PDA/SA-ZIF-8.

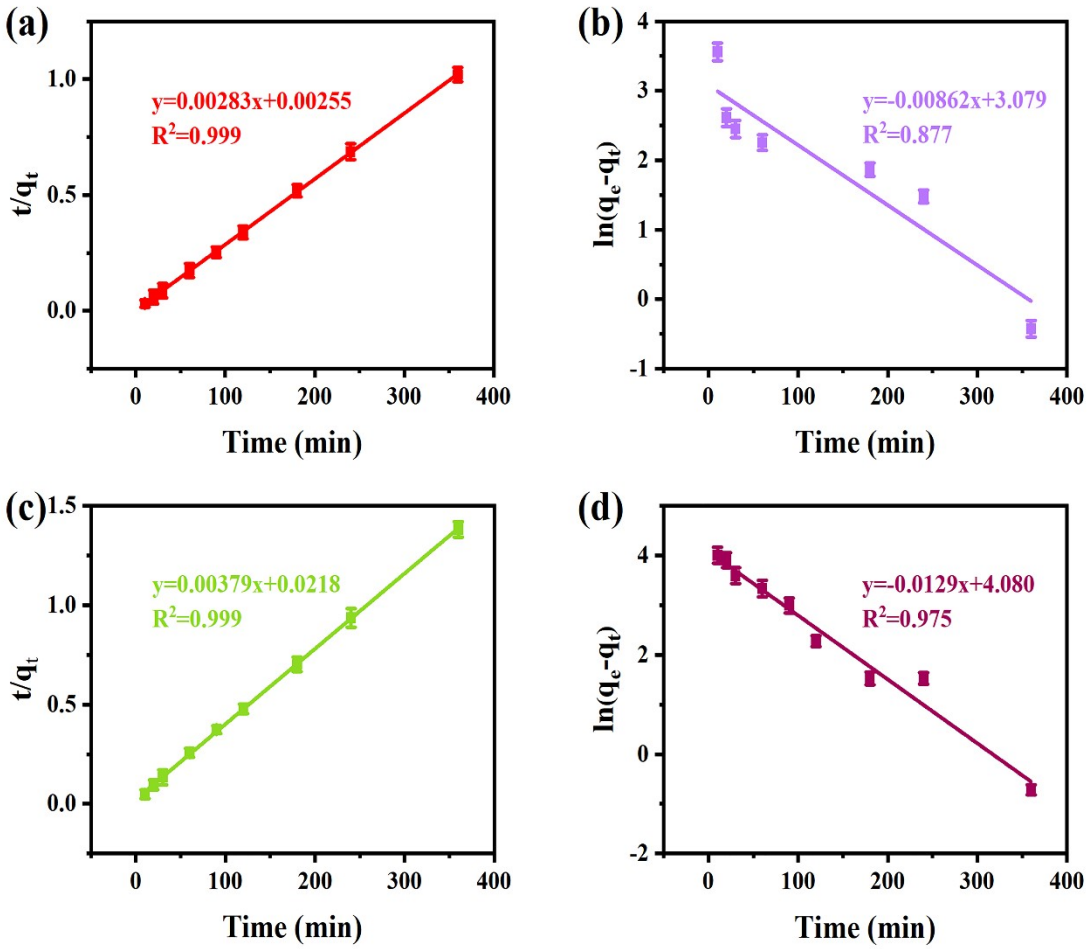

Fig. S6 (a) The Pseudo-second-order kinetic and (b) Pseudo-first-order kinetic model fittings for uranium adsorption on the H-PDA/SA-ZIF-8. (c) The Pseudo-second-order kinetic and (d) Pseudo-first-order kinetic model fittings for uranium adsorption on the PDA/SA-ZIF-8.

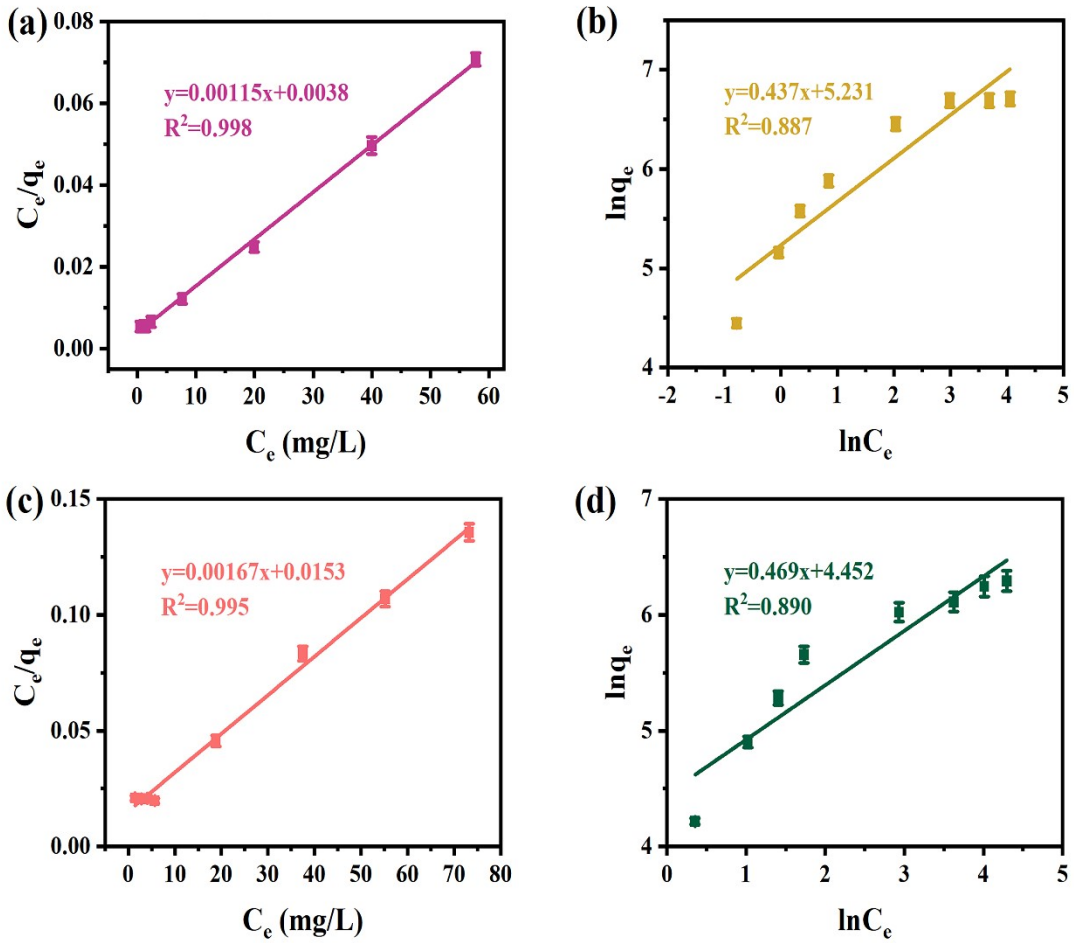

Fig. S7 The (a) Langmuir and (b) Freundlich model isotherm linear regression fitting for uranium adsorption on the H-PDA/SA-ZIF-8. The (c) Langmuir and (d) Freundlich model isotherm linear regression fitting for uranium adsorption on the PDA/SA-ZIF-8.

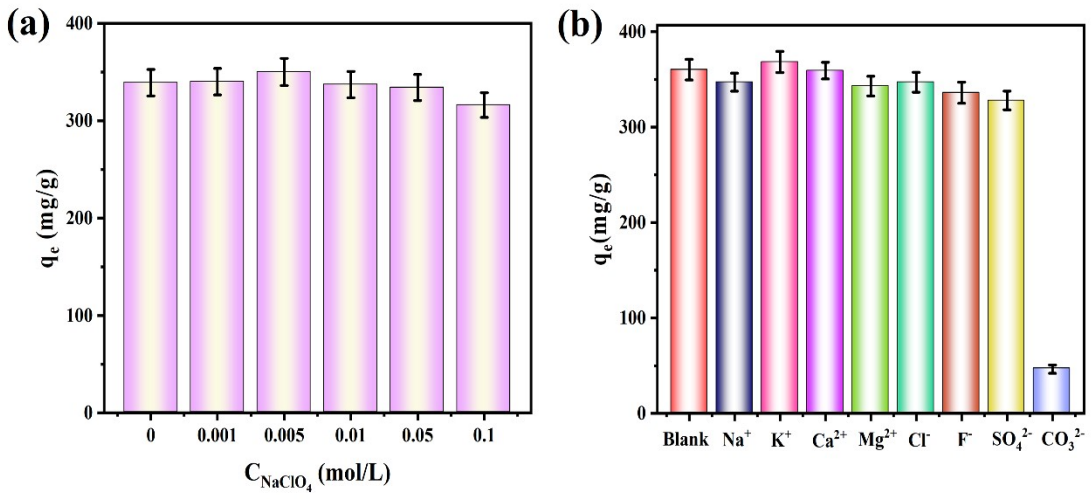

Fig. S8 (a) Effect of ionic strength on uranium adsorption capacity of H-PDA/SA-ZIF-8. (b) Effect of different ions on uranium removal for H-PDA/SA-ZIF-8.

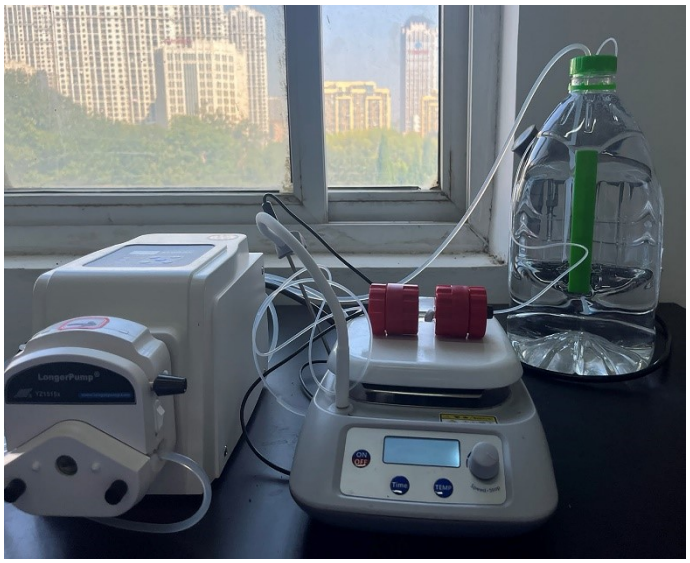

Fig. S9 Schematic of equipment used for uranium extraction from natural seawater by H-PDA/SA-ZIF-8. (The H-PDA/SA-ZIF-8 was placed in the chromatographic column and the 0.22 μm filter paper was placed on both sides to avoid the loss of the H-PDA/SA-ZIF-8. The seawater was circulated through the pump to realize uranium extraction from seawater.)

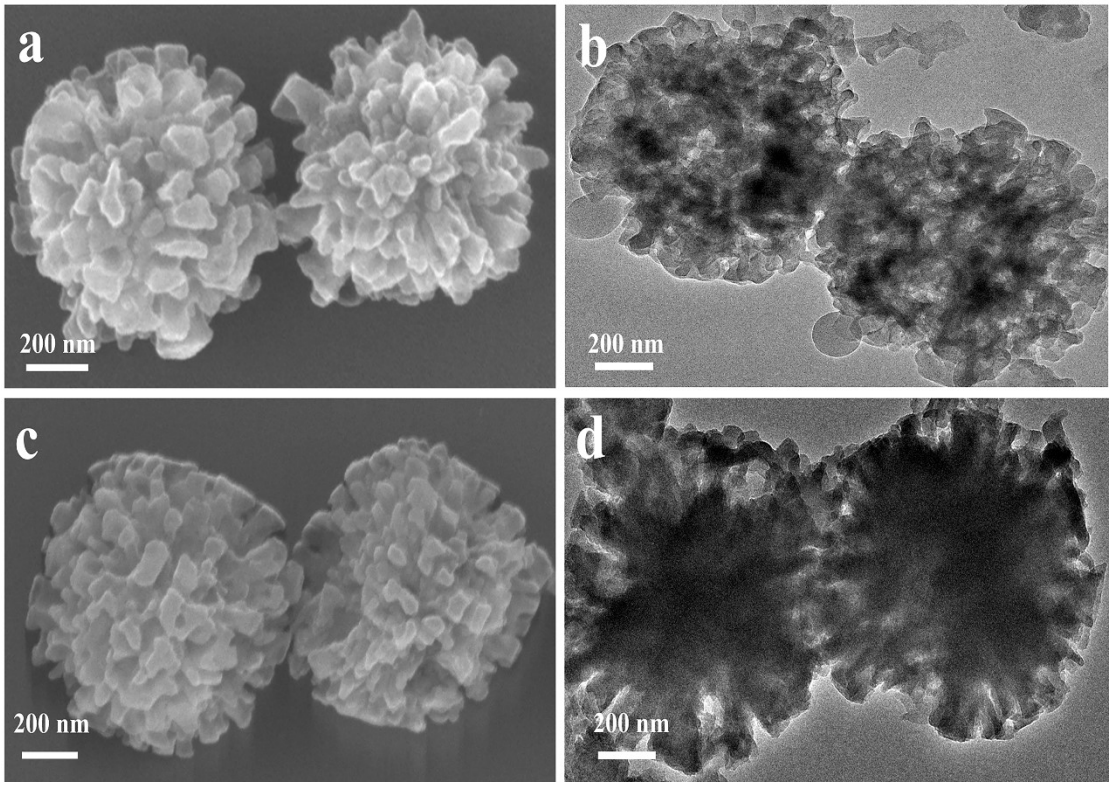

Fig. S10 SEM and TEM images of (a, b) H-PDA/SA-ZIF-8 and (c, d) H-PDA/SA-ZIF-8-U.

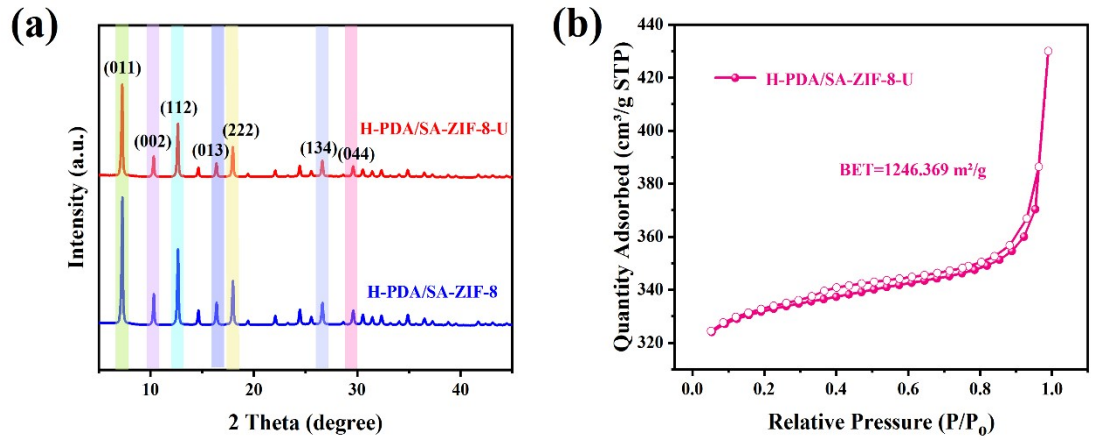

Fig. S11 (a) The XRD analysis of H-PDA/SA-ZIF-8, and H-PDA/SA-ZIF-8-U. (b) N_2 adsorption/desorption isotherms of H-PDA/SA-ZIF-8-U at 77 K.

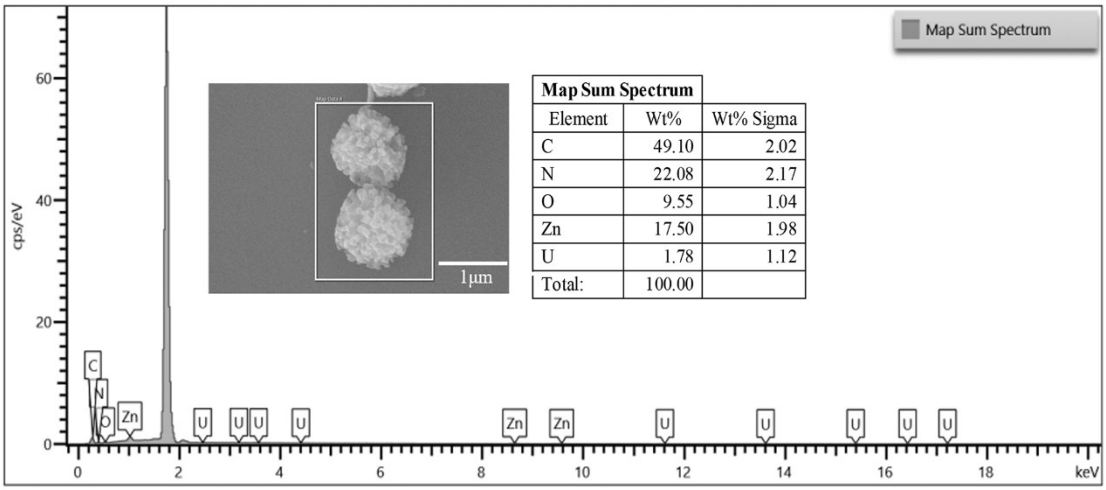

Map Sum Spectrum		
Element	Wt%	Wt% Sigma
C	49.10	2.02
N	22.08	2.17
O	9.55	1.04
Zn	17.50	1.98
U	1.78	1.12
Total:	100.00	

Fig. S12 The SEM micrographs and SEM-EDS spectrum of H-PDA/SA-ZIF-8-U.

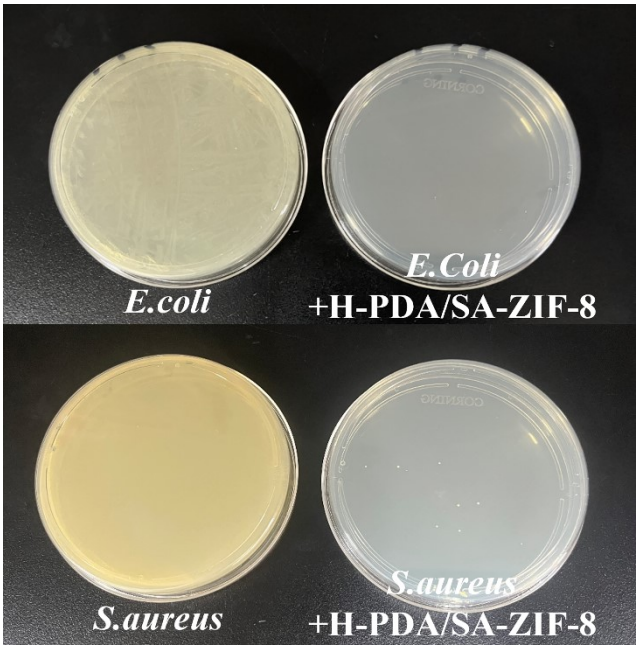

Fig. S13 Antibacterial activity against *E.coli* and *S. aureus*.

Table S1 Specific surface area and pore volume parameters for PDA/SA-ZIF-8 and H-PDA/SA-ZIF-8.

Samples	Specific surface area ($m^2\ g^{-1}$)	Pore volume ($cm^3\ g^{-1}$)
PDA/SA-ZIF-8	1077.83	0.4517
H-PDA/SA-ZIF-8	1234.92	0.6751

Table S2 The Pseudo-second-order and Pseudo-first-order kinetics parameters onto H-PDA/SA-ZIF-8, PDA/SA-ZIF-8.

Adsorbent	Pseudo-second-order model			Pseudo-first-order model		
	q_e ($mg\ g^{-1}$)	k_2 ($g\ mg^{-1}\ min^{-1}$)	R^2	q_e ($mg\ g^{-1}$)	k_1 (min^{-1})	R^2
PDA/SA-ZIF-8	263.9	6.60×10^{-4}	0.999	59.2	1.29×10^{-2}	0.975
H-PDA/SA-ZIF-8	353.4	3.37×10^{-3}	0.999	21.7	8.62×10^{-3}	0.877

Table S3 The Langmuir and Freundlich model parameters onto H-PDA/SA-ZIF-8, PDA/SA-ZIF-8.

Adsorbent	Langmuir model			Freundlich model		
	q_m (mg g^{-1})	k_L (L mg^{-1})	R^2	k_F (L g^{-1})	n	R^2
PDA/SA-ZIF-8	598.8	0.109	0.995	85.8	2.132	0.890
H-PDA/SA-ZIF-8	869.6	0.306	0.999	186.9	2.288	0.887

Table S4 Thermodynamic parameters of uranium adsorption on H-PDA/SA-ZIF-8.

ΔH^0	ΔS^0	ΔG (kJ mol^{-1})		
(kJ mol^{-1})	(J mol^{-1} K^{-1})	298.15 K	308.15 K	318.15 K
211.920	740.686	-9.162	-15.792	-24.011

Table S5 Concentrations of uranium and competing metals in natural seawater (SW) and simulated seawater.

Element	U	Fe	V	Co	Cu	Zn	Pb	Ba
Natural Seawater (ppb)	3.3	1.0-2.0	2.2	0.06	1.3	4.1	0.7	30
Simulated Seawater (ppb)	330	200	220	6	130	410	70	300

Table S6 Comparison of the performance of different adsorbents for uranium extraction from natural seawater.

Adsorbents	q_e (mg g^{-1})	Time (d)	Ref.
MIL-101-OA	4.60	5	4
Anti−UiO−66	4.62	30	5
COF-HHTF-AO	5.12	25	6
UiO-66-NH-(AO)	5.20	8	7
ZIF-67@SiO_2-A/PAM	6.63	30	8
c-PVA-g-PAO&MXene NFs	2.23 (light) 1.76 (dark)	7	9
AO-PAM/Alg	6.23	20	10
H-PDA/SA-ZIF-8	6.9	15	This work

Table S7 Specific surface area and pore volume parameters for H-PDA/SA-ZIF-8 and H-PDA/SA-ZIF-8-U.

Samples	Specific surface area (m^2 g^{-1})	Pore volume (cm^3 g^{-1})
H-PDA/SA-ZIF-8	1234.92	0.6751
H-PDA/SA-ZIF-8-U	1246.37	0.6651

Table S8 The calculated structural parameters of UO_2^{2+} and three coordination modes towards UO_2^{2+}.

Complex	Bond length			E_{ads} (kcal mol^{-1})
	U-O (Å)	U-N (Å)	U-O_{ax} (Å)	
UO_2^{2+}			1.741	
oxime type N and oxime type O	2.53	2.41	1.752	-55.24
hydroxyl type O	2.42		1.753	-17.41
oxime type N and hydroxyl type O	2.51	2.48	1.750	-69.25

References

1 J. Xiong, B. Chen, Z. Gu, S. Liu, M.-H. Zong, X. Wu and W.-Y. Lou, *Chem. Eng. J.*, 2023, **468**, 143622.

2 W. Wang, Q. Luo, J. Li, Y. Li, R. Wu, Y. Li, X. Huo and N. Wang, *Chem. Eng. J.*, 2022, **431**, 133483.

3 D. Mei, L. Liu, H. Li, Y. Wang, F. Ma, C. Zhang and H. Dong, *J. Hazard. Mater.*, 2022, **422**, 126872.

4 H. Wu, F. Chi, S. Zhang, J. Wen, J. Xiong and S. Hu, *Microporous Mesoporous Mater.*, 2019, **288**, 109567.

5 Q. Yu, Y. Yuan, J. Wen, X. Zhao, S. Zhao, D. Wang, C. Li, X. Wang and N. Wang, *Adv. Sci.*, 2019, **6**, 1900002.

6 G. Cheng, A. Zhang, Z. Zhao, Z. Chai, B. Hu, B. Han, Y. Ai and X. Wang, *Sci. Bull.*, 2021, **66**, 1994-2001.

7 L. Ma, J. Gao, C. Huang, X. Xu, L. Xu, R. Ding, H. Bao, Z. Wang, G. Xu, Q. Li, P. Deng and H. Ma, *ACS Appl. Mater. Interfaces*, 2021, **13**, 57831-57840.

8 Y. Song, H. Tan, S. Qin, Z. Liu, C. Liu, C. Shen, P. Yang and S. Li, *Nano Res.*, 2023, DOI: 10.1007/s12274-023-6233-x.

9 C. Huang, M. Fu, L. Ma, C. Mao, Y. Yao, X. Xu, L. Xu, J. Han, X. Xue, G. Xu, M. Wu, H. Shao and H. Ma, *Chem. Eng. J.*, 2023, **474**, 145718.

10 X. Zhang, D. Li, C. Cui, S. Chen, M. Ji, W. Tang, L. Yang, F. Zhang, J. Li, D. Zhang and X. Xu, *Polym. Chem.*, 2023, **14**, 2902-2915.